Dissipation Within the Surface Mixed Layer

N. S. OAKEY AND J. A. ELLIOTT

Bedford Institute of Oceanography, Dartmouth, Nova Scotia, Canada B2Y4A2

(Manuscript received 26 March 1981, in final form 5 October 1981)

ABSTRACT

Observations of turbulent energy dissipation, ϵ, measured during a week-long mixed-layer study on the continental shelf off Nova Scotia are presented. This time series of dissipation measurements at a fixed site and with a wide range of wind speeds indicates that a constant fraction of the energy flux in the atmospheric boundary layer appears as dissipation in the mixed layer. Our measured velocity-shear spectra are consistent in shape with an isotropic-turbulence spectral form and simultaneous determinations of spectral level from two mutually perpendicular sensors are consistent with isotropy. Significant changes in turbulence levels between two profiles a few minutes apart are observed. These changes (often a factor of 10) emphasize the necessity of adequate space–time averaging to obtain good mean values of ϵ. Including data from measurements of the large-scale density and velocity fields, the generation of the observed turbulence is thought to be Richardson-number instabilities in the mixed layer rather than direct surface phenomena such as wave breaking.

1. Introduction

This paper presents the results of a study in which the rate of dissipation of mechanical energy in the "mixed layer" has been related to the energy input from the atmosphere. The various interactions which transfer energy between the atmosphere and the ocean generate surface waves, currents, and internal waves, and modify the density profile. Directly or indirectly, most of these processes will dissipate energy in the mixed layer. A knowledge of turbulent processes, including the dissipation of turbulent energy, is fundamental to our understanding of mixing and the distribution of heat and salt in the ocean. We find that dissipation in the mixed layer accounts for a constant fraction of the energy flux in the atmospheric boundary layer.

The dissipation, ϵ, was determined from the measurement of vertical profiles of velocity microstructure to dissipation scales using the instrument OCTUPROBE II (Oakey, 1977). Over the nine-day period from 28 September to 6 October 1976, ϵ was determined at $\sim$6 h intervals for the mixed layer and upper pycnocline at the experimental site (Fig. 1) near Emerald Basin on the Scotian shelf.

The choice of Emerald Basin was a compromise between an easily accessible location where a ship could be moored and an experimental area where to a first approximation the density profile was constant horizontally. By avoiding areas where there are 'oceanic fronts' in the surface layer, we have collected data in an area where the major energy input to the turbulent structure is through surface stress and not horizontal processes. In this sense the experiment should be representative of processes that occur in the surface layers of most of the oceans.

The earlier work on surface layers has been reviewed recently in the book edited by Kraus (1977). Most of the earlier studies were limited to measuring the vertical density profile and they concentrated on predicting the depth of the mixed layer. There have been, however, some direct measurements of dissipation. Stewart and Grant (1962) measured dissipation rates in the near-surface (1 m to 15 m) using hot-film anemometer techniques. They were concerned with wave dissipation and concluded that most occurred within a wave amplitude of the surface. More recent results have been published by Osborn (1978) using instrumentation similar to our own. Although he concentrated on deeper layers, he did observe "a region of relatively high dissipation rate associated with the bottom of the mixed layer." Dillon and Caldwell (1980) calculated dissipation rates in the upper ocean during the Mixed Layer Experiment in the Pacific using the temperature-gradient spectrum and found a "dramatic contrast in turbulence between low and high wind speed periods."

2. Overview and velocity microstructure measurement

a. *Emerald Basin experiment*

The Emerald Basin experiment was designed to study processes in the mixed layer and in the pycnocline. This paper discusses the results from the

0022-3670/82/020171-15$07.75

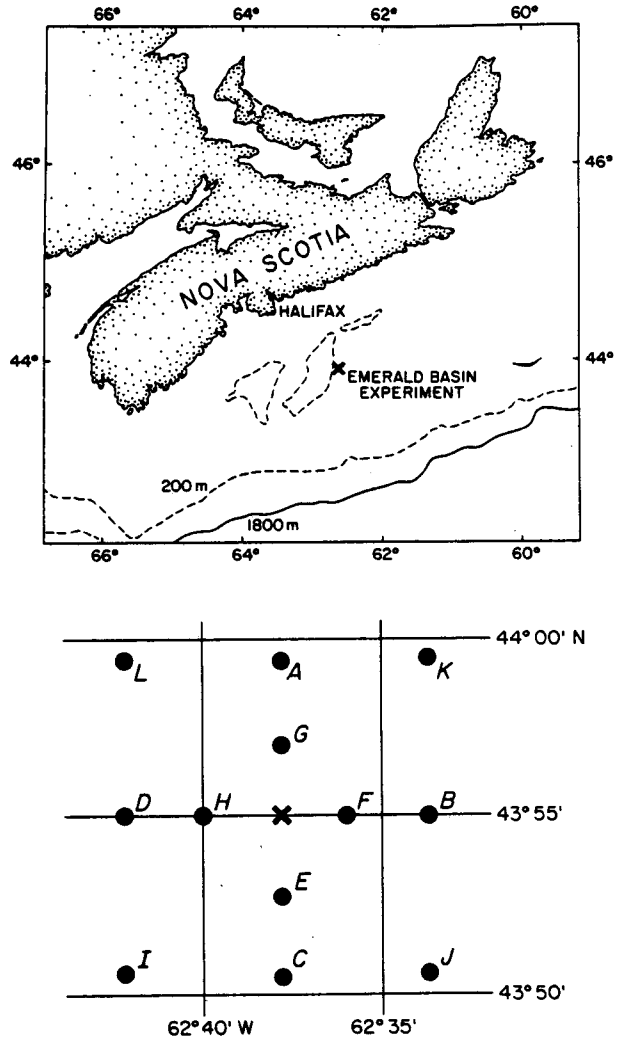

FIG. 1. Location of the Emerald Basin Experiment. The site plan with a central current meter mooring (x) is given below; the lettered points are CTD station positions.

mixed-layer part of the study only. To obtain a time series of the larger-scale water motions, a mooring was placed at the center of the study area at (43°55'N, 62°38'W) on the eastern edge of Emerald Basin (Fig. 1). It consisted of two Aanderaa current meters and two thermistor chains in a taut mooring with a subsurface float at a depth of 10 m in a water depth of 195 m. The upper Aanderaa current meter was at a depth of 12 m (in a 20 m deep mixed layer) with a 33 m thermistor chain spanning the depth below to a second Aanderaa RCM at 46 m in the pycnocline; below this was a second thermistor chain. Other data were collected from the ship CSS *Dawson* which, for the majority of the time, was anchored (see Fig. 1) within 4 km of the mooring to the south or southeast.

The observational program on board the ship was scheduled to yield overlapping time-series of vertical profiles of microstructure using OCTUPROBE II; temperature, salinity, depth profiles using a Guildline CTD; and measurements of large-scale horizontal-velocity shear using a profiling Aanderaa current meter. The frequency of observations varied because of weather and maintenance constraints but we obtained an average of about four measurement repetitions per day, as well as special intense sets of observations. On five occasions, a CTD survey was conducted at the grid of stations around the site shown in Fig. 1. These surveys were done to identify the horizontal variability at the site.

OCTUPROBE II (Oakey, 1977) is shown schematically in Fig. 2. This instrument is a 2 m long free-fall device with a variety of small-scale and microstructure sensors as well as pressure and acceleration sensors. The microstructure sensors (temperature, conductivity and velocity shear), are located on stings well ahead (~0.4 m) of the main vehicle body. In this exposed position, they are not affected by eddies shed by the vehicle or significantly by blockage. They are, however, vulnerable to damage, particularly on deployment and recovery. The instrument falls at a nominal speed of 0.5–0.6 m s^{-1}, trailing a light line used for easy recovery and rapid redeployment. The instrument drop speed tends to

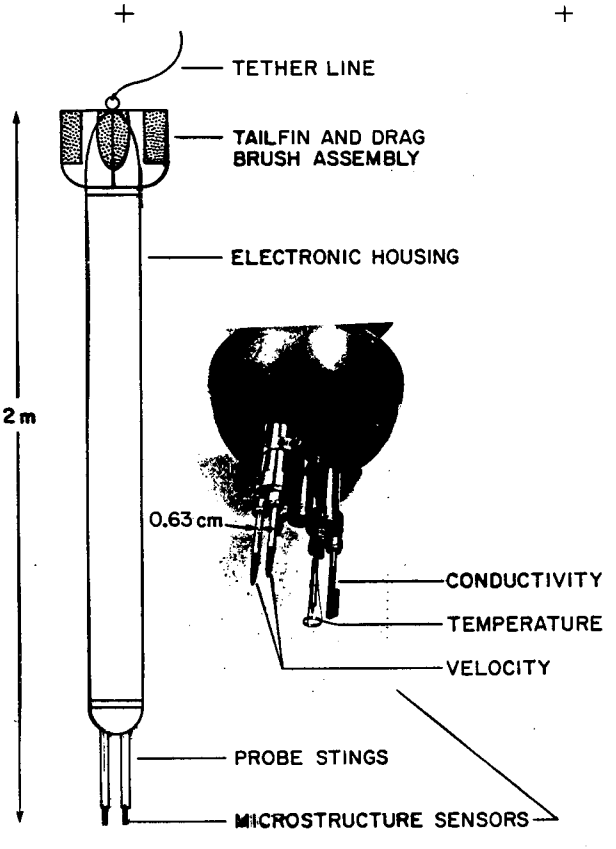

FIG. 2. The vertical-microstructure profiler OCTUPROBE II.

decrease with depth because of increased line drag and increasing buoyancy as water density increases. The internal recording of data in FM–FM format is limited to ~25 min so a typical OCTUPROBE station consists of four to six profiles to 100 m before the final on-board recovery.

A detailed description of the electronic and probe specifications for each parameter measured by OCTUPROBE has been given by Oakey (1977). A summary of the principal sensors used is given here. A detailed description of the velocity-microstructure sensors which are the main focus of this study is given at the end of this section.

Sensors on OCTUPROBE are:

1) two velocity-shear probes to measure two components of velocity microstructure perpendicular to the direction of travel of OCTUPROBE;
2) a thin-film thermometer (DISA model 55R46) to obtain temperature-gradient microstructure; both the temperature signal and the gradient signal (obtained electronically using a 6 dB per octave filter) were recorded separately;
3) a four-terminal conductivity sensor to monitor scales of 5 cm or larger; because of calibration problems it was not used to calculate density or density gradient;
4) a pressure sensor to monitor depth with a net accuracy equivalent to ±0.5 m;
5) three mutually perpendicular accelerometers to monitor high-frequency vehicle motion in the range of interest.

An attempt was made to monitor the mean shear of the horizontal velocity at the experimental site using a profiling Aanderaa current meter. The profiles, taken in conjunction with the data from the two moored current meters, were used to identify the variation with depth of the velocity shear. The method involved lowering a weighted cable to a depth of 100 m over the side of the anchored ship. A current meter at the bottom of the cable gave an indication of the ship's motion relative to the water during the observation period. A second Aanderaa current meter, attached to a float but with slightly negative buoyancy, was allowed to free-fall down the cable at a speed of 0.1 m s^{-1}. With a sampling period of 30 s, the profiling meter had a vertical spatial resolution of ~3 m. The records from the vertical-profiling meter and bottom meter were subtracted vectorially to give the velocity profile with respect to 100 m. The accuracy of the magnitudes of the difference vectors is estimated to be ±0.02 m s^{-1} from the RMS difference between profiling and bottom meter in the bottom 25 m of the profile.

Throughout the experiment, standard meteorological observations were collected on board the ship. Our main concern was with the windspeed observations. Even with an accurate anemometer, blockage by the ship can introduce substantial errors. To check for blockage errors, the CSS *Dawson* was calibrated in the Bedford Basin, adjacent to the Bedford Institute of Oceanography (Elliott, 1981). With the ship located near the center of the Basin, wind speeds were monitored on board the vessel at different headings simultaneously with measurements from a small workboat fitted with an anemometer on top of a 10 m mast. Blockage on the workboat was negligible. The shipboard measurements showed blockage errors of −20% to +20% for a range of azimuths 50° to port to 50° to starboard respectively. Throughout most of the Emerald Basin experiment with the ship at anchor, the wind direction was within this range of headings.

Throughout the experiment, there was a slow drop in temperature from about 17.5 to 15.5°C for all thermistors of the upper chain in the mixed layer. Superimposed on this was the rise and fall of temperature which corresponds to the daily heating and cooling cycle, with an amplitude of less than one-half a degree.

b. Velocity microstructure sensors

Horizontal velocity shear is measured using a probe originally designed by Siddon (1971) for use in air and later adapted by Osborn and Siddon (1975) for use in water. It has been described in detail in the recent article by Osborn and Crawford (1980). The probes used in the present study were fabricated at the Bedford Institute (Oakey, 1977) and for the remainder of this paper will be referred to simply as shear probes.

Shear probes use a piezobimorph beam to sense the lift produced on an axisymmetric foil of revolution by a turbulent velocity fluctuation, u, perpendicular to its axis as the probe moves through the water at a mean speed, V. Two probes are used to measure two components of velocity shear. The voltage output of the sensor is given by

$$E_0(t) = S_v \rho V u(t), \tag{2.1}$$

where S_v is a calibration factor, ρ is the density of water, V the mean flow speed, and $u(t)$ the turbulent off-axis flow. Making use of the nearly constant vertical drop speed V, and using Taylor's hypothesis, the velocity shear is given by

$$\frac{du}{dz} = \frac{1}{V^2 \rho S_v} \frac{dE_0(t)}{dt}. \tag{2.2}$$

Each shear probe used in the experiment was calibrated before and after the cruise. This was carried out by holding the probe in a laminar jet and oscillating the probe through fixed known angles and using Eq. (2.1). The laboratory calibration repeatability was typically better than ±5%, and precruise and postcruise calibrations were typically within this

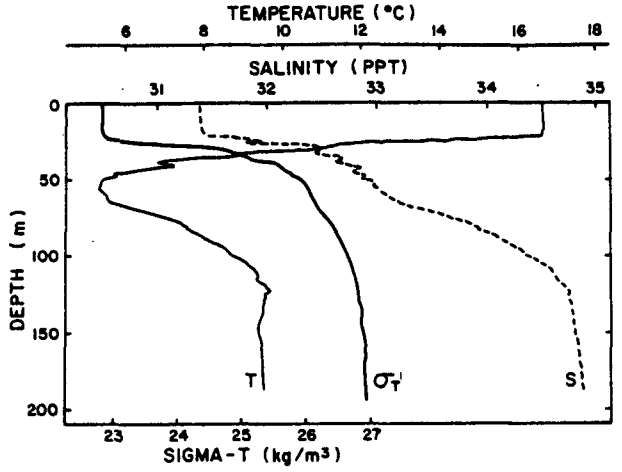

FIG. 3. Temperature; salinity; and σ_t depth profiles typical of the Emerald Basin area.

error. The absolute accuracy of the calibration may be somewhat worse because of systematic errors from effects such as flow separation as the probe is oscillated in the jet. Probes were monitored throughout the cruise using a simple spring balance to check for damage and were retired if suspect.

During the experiment the derivative of the velocity signal was recorded and converted to horizontal-velocity shear in the analysis using Eq. (2.2). The equivalent noise level of shear probes and OCTUPROBE expressed as dissipation per unit mass is 2×10^{-10} m^2 s^{-3}. The limitation at high turbulence levels is the ability of the sensor to resolve fluctuations in velocity which are small in scale compared to the physical dimensions of the sensor. For our probes we assume a single-pole cut-off form with a cut-off scale which is consistent with 2 ± 1 cm. The errors associated with this are discussed later.

3. Large-scale variability

The measurements of dissipation were the main focus of the experiment but a description of the large-scale temporal and spatial variability in temperature, salinity, density and velocity is important as a framework for interpreting these measurements of dissipation.

The selection criterion for the experimental site was that horizontal variations in the temperature, salinity and density should be small so that advective effects would not mask changes in the mixed layer from atmospheric forcing. Over a horizontal distance of 6 km (the range of our CTD surveys), it was a region without strong horizontal density structure or "fronts". A typical plot of temperature, salinity and σ_t versus depth (Fig. 3) from a CTD lowering midway through the experiment shows profiles characteristic of this area. There is a well-defined mixed layer to a depth of 20 m with very uniform temperature. There are, however, density gradients in the "mixed layer" resulting from a small persistent salinity increase towards the base of the mixed layer.

The temporal variability in the current speed and direction was obtained from the two current meters in a taut mooring with a subsurface float at 10 m depth at the center of the experimental array. The upper meter at 12 m depth in the mixed layer showed speeds of 0.3–0.5 m s^{-1}, with stronger currents during periods when the wind speed was higher. The variability was dominated by motions at the inertial period. The lower instrument, at 46 m, showed variability at the same frequency but with lower amplitude. The rate and direction difference between the upper and lower meters is shown in Fig. 4. It indicates a persistent shear of 0.2–0.6 m s^{-1} between the mixed layer and the pycnocline varying in direction at the inertial period. This indicated shear may be higher than in reality because of the effect of waves on the mooring and on the Aanderaa current meter at 12 m. At 12 m depth for a significant wave height of 2 m and a period of 6 s, typical of the 10 m s^{-1} winds during the experiment, the calculated orbital wave speed is 0.25 m s^{-1}. The indicated shear may be high by some fraction of this.

The progressive vector diagram for the current

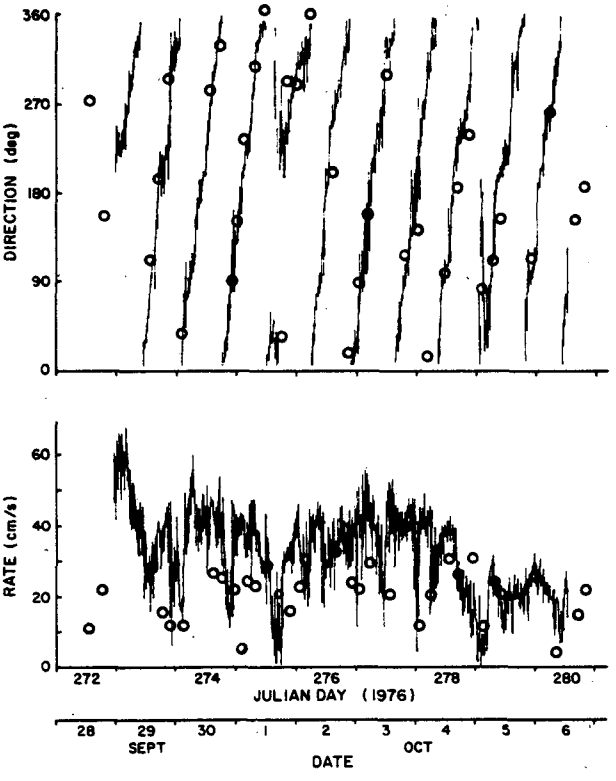

FIG. 4. Vector difference between velocities at the upper and lower current meters in the mooring, presented as rate and direction. The circles indicate the corresponding rate-direction differences obtained using a profiling current-meter pair.

meter in the mixed layer (Fig. 5) indicates a general northwesterly mean flow of 0.05 m s^{-1} on average over the experiment. Days 275 and 276 had higher mean currents of 0.14 m s^{-1}, while near the end of the experiment the mean flow was ~0.02 m s^{-1}. At the times indicated by the numbers 1–5 on Fig. 5, CTD surveys were made at the various sites indicated in Fig. 1. One salinity section, number 5, obtained near the end of the experiments using sites I, E, Mooring, F, K is shown in Fig. 6. There is considerable salinity variation in the mixed layer along this section but little temperature variation. The base of the mixed layer, defined by a significant large-scale temperature gradient, is indicated by a dashed line. Density gradients in the surface mixed layer are therefore determined largely by salinity. From five sections similar to that in Fig. 6, assuming that the current is advecting the salinity field through the site, and making use of the progressive vector diagram to fix the sections relative to one another, we have constructed (Fig. 7) a somewhat schematic picture of the salinity structure at 10 m for the study area. The orientation and length of each of the five CTD sections is indicated by dashed lines near each numbered dot.

At the fixed-experiment site where the ship was anchored, the variability observed in successive CTD

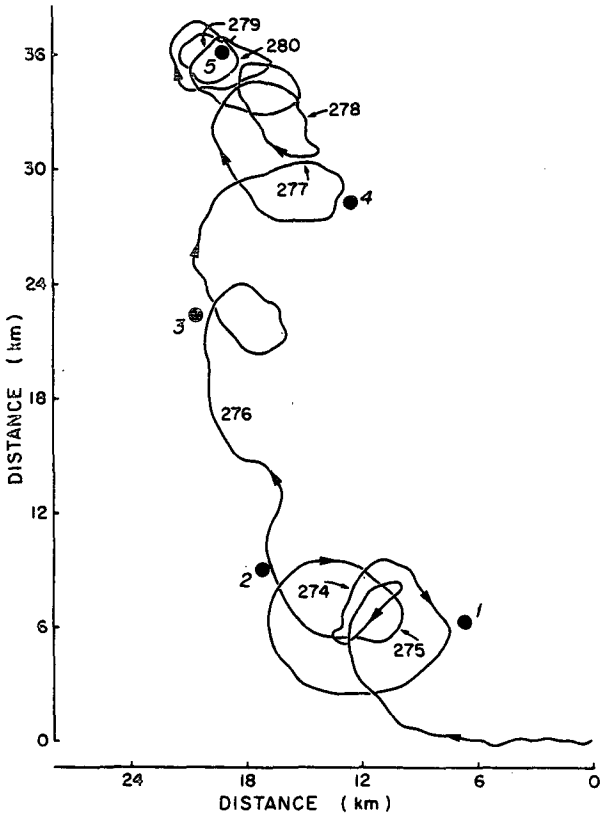

FIG. 5. Progressive vector diagram for the upper current meter.

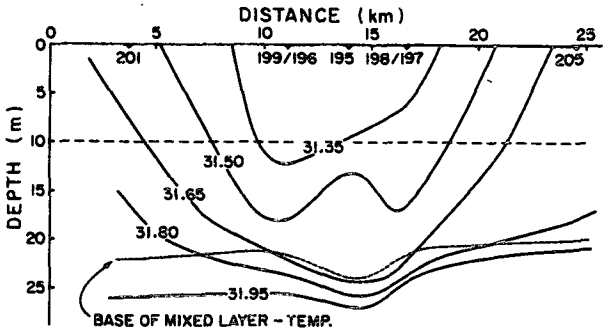

FIG. 6. Salinity section number 5. The dotted curve is the base of the mixed layer based on the temperature. The salinity at 10 m (the reference dashed line) is used in constructing the salinity field of Fig. 7.

profiles was a result of this salinity (and temperature) field being advected past us. The salinity time series is shown in Fig. 8. There are large salinity changes accompanied by small temperature variations; resultant vertical density gradients have values typically between 0.02 and 0.06 kg m^{-4} in the mixed layer at depths of 15 m. The dotted line in Fig. 8 is the mixed-layer depth based only on the temperature profile.

From the current-meter data, we know there is a mean shear between the mixed layer and the pycnocline. The two Aanderaa current meters used as a profiling pair allowed us to estimate the shear and its vertical location. The vertical resolution for this method with a sampling interval of 30 s and drop speed of 0.1 m s^{-1} was ~3 m. The average rate and direction for each profile were determined at the current-meter mooring depths of 12 and 46 m and compared with the moored instrument results. These data are shown as circles superimposed on the fixed-current-meter data of Fig. 4. The agreement is excellent in direction, but the data indicate, on the average, a rate 25%–50% smaller than at the mooring. The reason for this discrepancy is not clear. The response of the profiling instrument to waves may be very different from that induced in the moored instrument. Aside from this rate discrepancy, the profiling meter does indicate the velocity profile, and, because it is not affected by mooring motion, it may be more accurate than the fixed meters.

From the nearly 100 velocity profiles during the 10-day experiment, there is no universal profile. Fig. 9 indicates the three major types of profile observed. About $\frac{1}{5}$ of the profiles are similar to 9A, and show little shear in the mixed layer with a strong shear near the base extending into the pycnocline. A larger portion (~$\frac{1}{2}$) have a profile similar to 9B (with variations), again showing a strong shear near the base but with strong shear in the mixed layer as well. Others (~$\frac{1}{5}$) are similar to 9C, and show the majority of the shear in the mixed layer with little shear

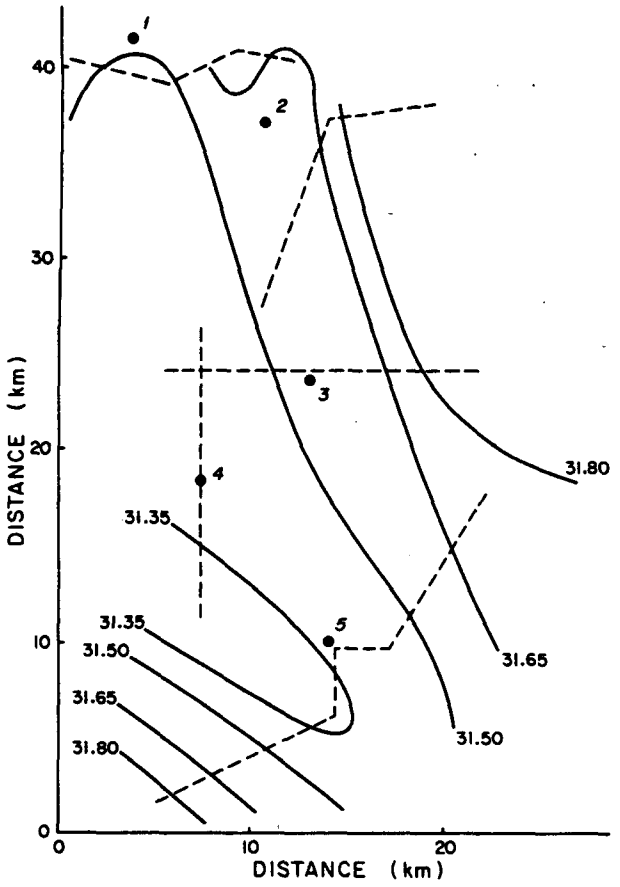

FIG. 7. Salinity at 10 m for the Emerald Basin study area.

below the base. For each profile in Fig. 9 the velocity-difference vectors used to calculate shear are indicated at the right, with zero degrees referenced up.

For each velocity profile, the density profile from the CTD nearest in time (0.5–1 h typically and indicated in the second plot of Fig. 9), was used to make an estimate of the 5 m vertical-averaged gradient Richardson number, Ri. Examples of this calculation are indicated in Fig. 9 in the third trace. In the upper 10 m, density gradients which are small compared to the resolution of the CTD, as well as possible near-surface wave effects causing errors in the current meter readings, may make these values of Ri unreasonably low. There are, however, many values of Ri of order 1 in the mixed layer and near the base of the mixed layer.

An error analysis for the calculation of Ri is difficult and not altogether convincing. There are two error sources associated with the calculation: the mean density gradient and the mean velocity shear. Because of the stability of the density profile in time, the latter error is assumed to predominate. A measurement precision of ± 0.02 m s^{-1} gives an estimated error in shear of 0.004 s^{-1} for the 5 m interval, typical of the minimum values of Fig. 9. For the upper 25 m, where the measured shear is >0.01 s^{-1} on average, this represents an error of a factor as large as 2–3, where the estimates of Ri are probably low if rotor pump-up is a problem. Deeper, where the error estimate is comparable to the measured mean shear, the error bars are very large.

A summary of the Richardson-number data (Fig. 10) shows the histogram of occurrences of values of Ri at each 5 m depth interval for the 100 profiles. Most of the values less than the critical value of 0.25 occur in the mixed layer. There are many small values even in the pycnocline. In an attempt to estimate where shear instability may cause turbulence and mixing, the mean depth (Fig. 8) for each profiling-current-meter station above which Ri < 1 was estimated. These depths have been plotted on Fig. 8, along with the salinity time series. The solid curve in Fig. 10 is the median value of Ri as a function of depth for the experiment. It has a value of ~ 4 at the base of the mixed layer. The depth above which Ri < 4 was computed for each station and is plotted on Fig. 8 for comparison with the depths above which Ri < 1. During all of the earlier part of the experiment, when the winds were highest, the depth above which Ri < 1 or Ri < 4 was nearer the base of the mixed layer than later in the experiment, when the

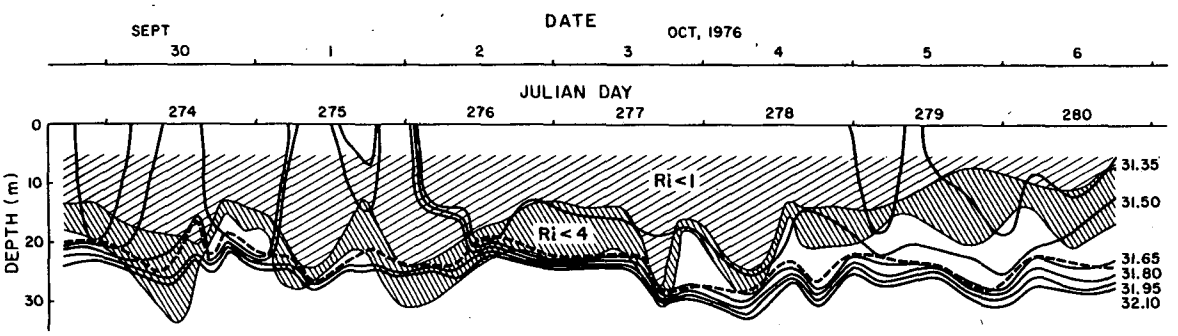

FIG. 8. The salinity time series at the fixed Emerald Basin observation site. Superimposed is (crosshatching) the depth interval in which Ri < 1 and (heavy crosshatching) the region where $1 \leq$ Ri < 4. The dashed line is the mixed-layer depth determined from the CTD temperature record.

winds were lower. It is interesting to note the suggestion of a periodic variability in the depth above which Ri < 1 which lasts 18–20 h and is approximately the same as the inertial period which is 17 h. It is also striking that, towards the end of the experiment (after day 278), the depth of the region

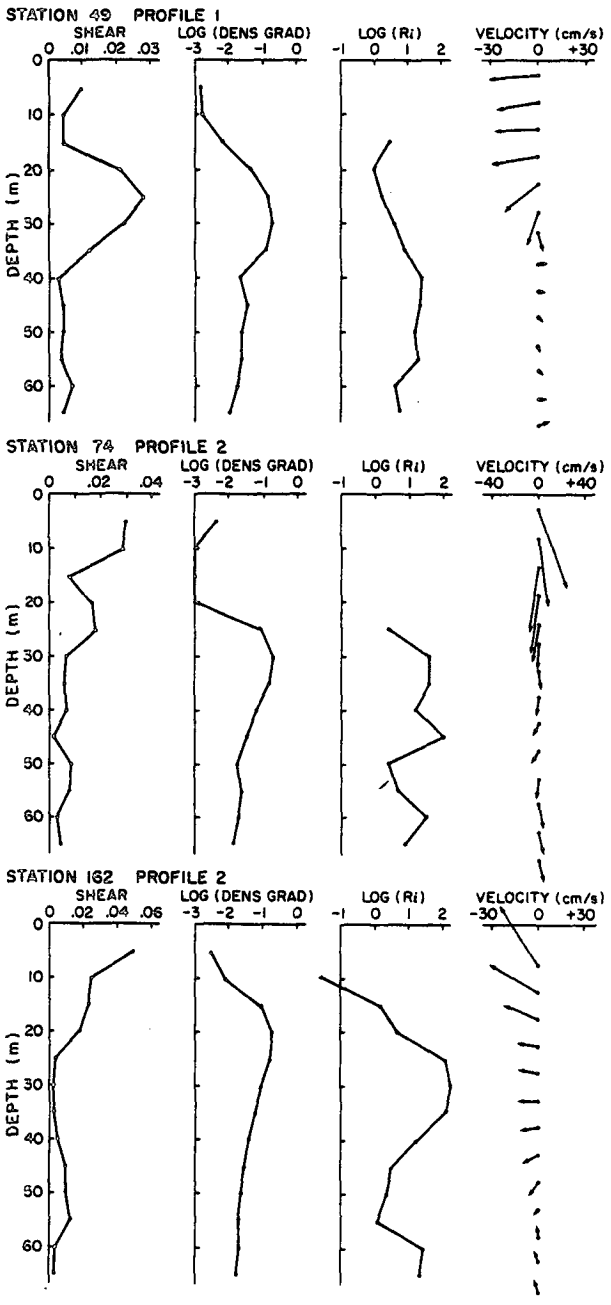

FIG. 9. Determination of the gradient Richardson number Ri (5 m average) from the profiling current meter and CTD. Vector differences between the profiling current meter and a reference RCM at 100 m are shown to the right (with the magnitude defined by the abscissa and with North referenced up). From left to right are shown: the corresponding shear, the density gradient obtained from the CTD, and the gradient Richardson number, Ri.

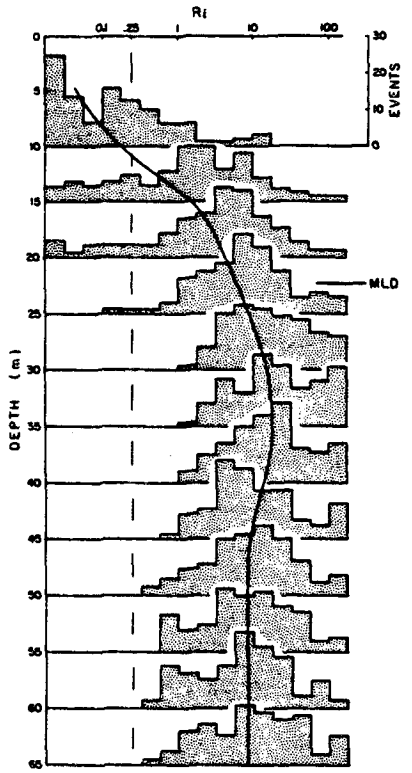

FIG. 10. Summary of the determinations of gradient Richardson number Ri at 5 m depth intervals for the 100 determinations made with the profiling Aanderaa current meter. The solid line represents the median values of Ri versus depth.

where Ri < 1 is only ~10 m. The Richardson number near the base of the mixed layer in this period when no deepening is occurring is much greater than 4.

4. Energy budget

The rate of dissipation of mechanical energy, ϵ, which we obtained from measurements during our experiment, is one of the components of the energy budget for the mixed layer. We have not attempted to measure or estimate all of the components of this budget and show a balance. Instead, we correlate dissipation levels to the gross parameters such as the mean wind speed. A detailed development and description of the energy-balance equation for the mixed layer is given by Niiler and Kraus (1977). A brief summary will be given here to provide a framework into which our measurements of ϵ can be fitted more clearly.

The turbulent-energy-budget equation is expressed in a simplified one-dimensional form by assuming all the fluxes are vertical (i.e., horizontal advection is assumed to be not important). For the experimental site chosen, this assumption is discussed below. For the fluctuating components of the flow, the equation is

$$\int_{-h}^{0} dz\Bigg[\underbrace{\frac{1}{2}\frac{\partial q^2}{\partial t}}_{(A)} + \underbrace{\overline{u'w'}\frac{\partial U}{\partial z}}_{(B)} - \underbrace{\overline{w'b'}}_{(C)} + \underbrace{\frac{\partial}{\partial z}\left(\frac{\overline{w'q^2}}{2} + \overline{w'p'}\right)}_{(D)} + \epsilon\Bigg] = 0, \quad (4.1)$$

where $q^2 = u'^2 + v'^2 + w'^2$ and $b' = -g\rho'/\rho$. The primed variables are perturbations from the mean for the density ρ, pressure p, and the velocity components u, v, w in the directions x, y and z, respectively. The mean horizontal velocity U is in the x–z plane (z is vertical). ϵ is the rate of dissipation of mechanical energy, h is the depth of the mixed layer, and g the acceleration of gravity.

Term (A) in Eq. (4.1) is the time-rate of change of the turbulent kinetic energy and is generally considered to be small (Niiler and Kraus, 1977). For our experiment, it is always less than 1% of ϵ. Term (B) is a source term resulting from the interaction between the turbulent Reynolds stress and the gradient of the mean flow; the third term (C) is the buoyancy flux which includes changes in the density profile. Terms (B) and (C) are generally considered to be source terms, although deepening of the mixed layer, which is part of (C), is an energy sink. The fourth and fifth terms (D) are flux-divergence terms which represent a redistribution of energy by turbulent advection and pressure-work, respectively. These terms could be a source at one depth if at another depth there is a concentrated dissipation mechanism. Such a mechanism might be high dissipation at the surface due to wave breaking, or at the base of the mixed layer as one would expect from the "slab" model concept. The final term, the dissipation ϵ, can have as a source of energy any or all of the other terms.

The assumption that advection is not important does not affect the accuracy of our determination of ϵ; it may affect the relative size of other terms in the energy-balance equation. From our limited spatial survey of density and, in particular, velocity, we are unable in this experiment to estimate all of the terms in Eq. (4.1). If the turbulent velocity fluctuations which we measure are generated in response to local wind forcing with time scales $< 10^4$ s (3 h), advection at 0.2 m s^{-1} yields a distance of 2 km which is small compared to the scale of the wind forcing. As shown in Fig. 6, horizontal gradients of salinity and density are three orders of magnitude smaller than vertical gradients. Advection of 2 km of this structure will change the "local" gradient at our measurement site only fractionally. On the other hand, time scales characteristic of dissipation, $(\epsilon/\nu)^{1/2}$, where ν is the viscosity, are of order seconds to tens of seconds. On these time scales, advection of turbulent energy is unimportant.

The dissipation is determined in our experiment from the vertical profiles of velocity microstructure measured with OCTUPROBE. The signal representing the local horizontal velocity is converted to a local vertical derivative by employing Taylor's hypothesis and substituting into the equation

$$\epsilon = \frac{15}{2}\nu\overline{\left(\frac{du'}{dz}\right)^2}, \quad (4.2)$$

where instead of u' we could also have used v'. Development of this equation depends upon the assumption of local isotropy of the turbulence (Hinze, 1959).

When discussing the total dissipation rate for the mixed layer, we will be referring to the integrated dissipation rate in the form

$$\epsilon_I = \int_{-h}^{0} \epsilon(z)dz, \quad (4.3)$$

where the integral is from a depth $-h$ at the base of the mixed layer to the surface at $z = 0$. In practice, dissipation in the top 5 m of this integral (about one-fourth of the total depth) must be estimated since OCTUPROBE data are not accurate in the top few meters. (This problem is discussed below.) The dissipation rate $\epsilon(z)$ in W m^{-3} makes ϵ_I, in W m^{-2}, the dissipation per unit area.

Eq. (4.3) may conveniently be used to compare the measured dissipation to the surface energy flux from the wind field. The energy flux from the atmosphere, which is a likely source of most of the dissipation observed in the mixed layer, can be estimated from the wind speed at a height of 10 m from

$$E_{10} = \tau U_{10} = \rho_a C_{10} U_{10}^3, \quad (4.4)$$

where ρ_a is the density of air, τ is the surface stress, $C_{10} = 1.3 \times 10^{-3}$ is the drag coefficient (Garratt, 1977) and U_{10} is the wind speed at 10 m height. This approach has been used by investigators such as Denman (1973) when studying the deepening of the mixed layer. Most of the energy flux, E_{10}, is dissipated in the air before reaching the sea surface and a small fraction is coupled across the air–sea interface. Richman and Garrett (1977) estimate that between 2 and 10% may cross the air–sea interface, including the energy going into the surface wave field. From studies by Denman and Miyake (1973) on deepening of the mixed layer, we know that 0.1–0.2% of E_{10} goes into potential energy of the mixed layer when deepening conditions exist. Little is known of the other terms in Eq. (4.1), except that an order-of-magnitude estimate of term (A), the change in kinetic energy of the fluctuating flow, indicates it to be small relative to other terms.

5. Dissipation analysis

a. Spectral analysis techniques

Dissipation levels were evaluated from the vertical profile signal by two different methods. One involved digitizing the analogue signal and computing a corrected dissipation spectrum for integration by digital techniques. This method is more accurate but more time-consuming than the second method. The second method uses an analogue spectrum analyzer, which is faster but less accurate.

The digital analysis technique included converting the velocity-microstructure-derivative signal from analogue to digital form at a sample rate of 1000 Hz, applying calibration factors indicated in Eq. (2.2), performing fast Fourier-transform analysis on blocks of 2048 points and averaging over those blocks contained in the depth segment being analyzed. The start and end depths of this segment were truncated to the nearest block, which corresponded to 0.5 m for the nominal drop speed of 0.5 m s^{-1} and the above sample rate and block size. The average spectrum for each profiling segment analyzed was corrected for instrument electronic frequency response and for the spatial averaging of the shear probe as described below. For each of the spectra, corrected for sensor and system response, the variance in velocity shear was obtained by integration. A corresponding dissipation was determined by using Eq. (4.2).

Within a section of data chosen for analysis, a large-magnitude signal—a spike—is occasionally observed which may be noise. These spikes may be caused by a shear probe striking an object in the water. The spikes, if they are obvious, are avoided in the analysis by ignoring the blocks of data containing them. Since the signal passed through the whole observing system, including the probe, separation of spikes from data on signal character alone is difficult. However, because there are two shear probe sensors measuring at once and the real signal tends to be isotropic, many spurious noise signals can be rejected because they are recorded by only one sensor.

The data selected for digital analysis were the first drop of each half-hour series of four or five profiles. The variation in signal level within a sequence was sufficiently large that a better variance estimate for the half-hour period could be obtained by analyzing all the data and averaging. For all of the profiles, the alternative method of analysis, a spectrum analyzer, was used. The data were block-averaged and corrected in the same way as they were for the digital technique. This alternative method was less time consuming, but less reliable because the available spectrum analyzer did not have as high a signal-to-noise ratio as the digital technique. This noise problem was more serious for low-level signals. Using the digital analysis as a control, the overall RMS deviation between the two methods was 20%, with the worst-case error (a factor of 2) being for low-signal-level data. Fortunately, for most of the half-hour sequences the worst-case errors are compensated by averaging with other more accurate and higher-level signals.

The confidence limit on the determined values of dissipation ϵ depends on a variety of factors. The uncertainty of the instrument drop speed, which was determined from a linear fit to the pressure signal, is ±5%, which leads to an error of ±10% in the measured velocity shear or ±20% in ϵ from Eq. (4.2). The uncertainty in the determination of the probe sensitivity S_v (±5%) leads to a further uncertainty of ±10% in ϵ while the errors in determining amplifier gains can contribute a further ±4%. The deviation from ideal frequency response of electronic circuits such as the 6 db octave^{-1} differentiator and analysis filters is applied at the spectral stage. The error in the power spectrum because of this correction is ±6% at 100 cycles m^{-1} and ±2% at 15 cycles m^{-1} (50 Hz and 7.5 Hz for V = 0.5 m s^{-1} respectively). Since ϵ is obtained by integrating the spectrum, this results in a spectral weighted error of ±3%. The error associated with correcting the spectra for the spatial resolution of the shear probe is poorly known. From geometrical considerations (Osborn and Crawford, 1980) and for a probe tip of 1 cm length, one estimates a cut-off scale λ_c = 2 cm. A preliminary study at the Bedford Institute comparing the shear probe to a thin-film x-probe indicated $\lambda_c = 2 \pm 1$ cm. A comparison with similar probes used by others is not directly applicable to our sensors which have slightly different geometry. Our choice is $\lambda_c = 2 \pm 1$ cm, with error bars based on the assumption that because of the probe's size λ_c cannot be <1 cm, and a variety of evidence such as our laboratory test leads one to believe it is <3 cm. In the determination of ϵ, the error resulting from the choice of λ_c is weighted at each wavenumber by the spectral variance at that wavenumber. Thus for $\lambda_c = 2 \pm 1$ cm, and assuming the response to be that of a single-pole filter, the error will be progressively larger at higher dissipations as the cut-off wavenumber becomes larger. The estimated error is 4% for $\epsilon = 10^{-9}$ m^2 s^{-3}, 10% for $\epsilon = 10^{-8}$ m^2 s^{-3}, 20% for $\epsilon = 10^{-7}$ m^2 s^{-3} and 36% for $\epsilon = 10^{-6}$ m^2 s^{-3} [obtained from convolving the "universal" spectral form of Nasmyth (1970) with the λ_c-correction-error curve]. Thus for most of the Emerald Basin experiment there is an uncertainty in the determination of ϵ of ~25% from this source alone. It should be emphasized that, since all the shear probes were of similar shape and construction, this is a systematic error. Consideration of all sources of error yields an uncertainty of ~60% maximum possible error (or ~35% RMS if the error sources are independent). Not included in this error estimate are the associated errors with the assumptions of isotropy that are im-

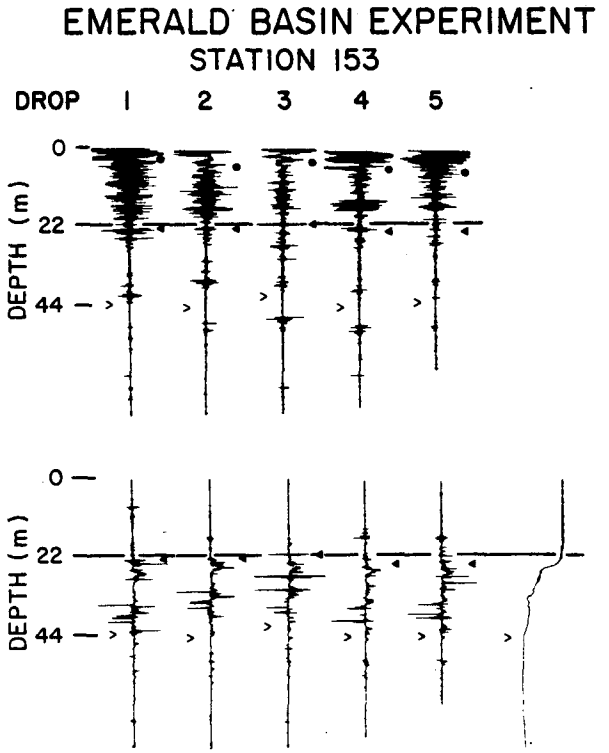

FIG. 11. Successive vertical-microstructure profiles to a depth of 50 m at 5-min intervals for Station 153. Velocity-microstructure gradient is shown above with full scale 0.5 (m s^{-1}) m^{-1}. The corresponding temperature gradient signals are shown below with temperature at the right. The mixed-layer depth is indicated by solid triangles, the depth below which we have analyzed the data by solid circles, and 44 m depth by arrows. The 22 m depth used as a reference is indicated by a dashed line.

plicit in Eq. (4.2), which alone may introduce a 50% error. Individual estimates of ϵ are therefore considered to be known within a factor of 2.

b. Dissipation data

The velocity-microstructure data analyzed to obtain ϵ are vertical profiles from OCTUPROBE. These were collected as series of four or five drops within a half-hour period that were repeated on average four times per day during the 10-day experiment. A visual examination of the analogue traces from these profiles reveals that any one profile can have significant variability in the vertical and can change considerably (by as much as a factor of 10) in average signal level from a lowering taken five minutes earlier. The changes over a half-hour series were not as large as those seen through the day or from day to day as the wind speed varied (Figs. 11 and 12). Fig. 11 is a sequence for Station 153 at ~5 min intervals. The plot is the signal from one of the velocity shear probes after passing through a differentiator. With a constant drop speed for OCTUPROBE, the signal is proportional to vertical gradient of velocity, normal to the sensor. Included for reference is the signal from a thin-film thermometer processed in a similar way. The mixed layer is considered to include depths down to the temperature microstructure that is correlated directly with the top of the thermocline.

An attempt was made in the study to avoid turbulence generated by the ship's wake. Our choice was to exclude all depths above 5.5 m, which cor-

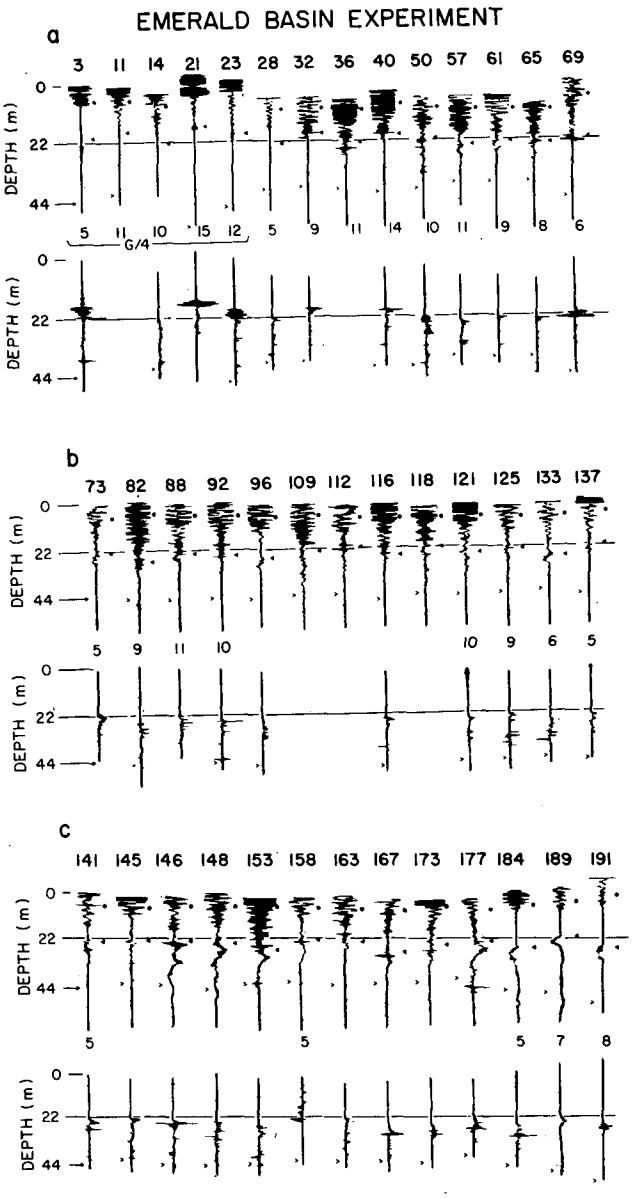

FIG. 12. The summary time series of velocity (above) and temperature microstructure (below) for the duration of the 10-day experiment. The format is the same as for Fig. 11. For each station the first (of four or five) profiles is given with the station number above and the wind speed below. Between stations 91 and 110 the wind speed was 10 m s^{-1} and from 141 to 184 near 5 m s^{-1}. The full-scale velocity gradient was ~0.5(m s^{-1}) m^{-1} for station 28 to the end and ~2(m s^{-1}) m^{-1} for stations 3–23 labeled G/4.

responds to a depth of 1.5 m below the draft of the ship. While precluding the study of data collected near the surface, this choice had the advantage that by the time OCTUPROBE reached this depth it was falling at its terminal velocity. OCTUPROBE does not always drop at the same speed—a result of changing buoyancy or changing drag from the nylon retrieval line. For this reason, in the diagrams, such as Fig. 11, the depth axis has been vertically adjusted so that all drops have a common reference at 22 m, a depth near the base of the mixed layer. In Fig. 11, closed circles mark the 5.5 m depth, closed triangles the mixed layer depth, and arrows the 44 m depth interval. Internal waves will cause the instantaneous mixed-layer depth to change; from the thermistor-chain and CTD data, a typical range is ≤ 3 m. Fig. 12 shows the series of velocity-microstructure data for the whole experiment, where the first profile of each half-hour series for one thrust sensor is shown. These profiles are marked in depth the same way as the profiles of Fig. 11.

Each microstructure profile in the mixed layer was divided into two parts for analysis. The lower part (lower mixed-layer) was the 10 m segment immediately above the pycnocline. The remainder (the upper mixed-layer) is the overlying segment below the near-surface delimiter at 5.5 m determined by the ship's hull. This upper mixed layer varied in thickness from 5 to 10 m. This artificial division into two depth intervals was adopted in the expectation that to extrapolate our measurements to the surface, the upper mixed-layer segment would be a better representation of the region (that we could not analyze) between 0 and 5.5 m than would the overall average.

A spectrum from one of the drops (Fig. 13) represents one of the best examples of high signal-to-noise ratio, which is the reason for choosing it. Two values of shear probe cut-off scale, λ_c, were used to correct the data, 2 and 1 cm, corresponding to 50 and 100 cpm, respectively. For the profiler speed of 0.5 m s^{-1}, these were equivalent to frequencies of 25 and 50 Hz respectively. The difference between the corrected spectra is small until one reaches scales corresponding to 50 cpm. Near the peak of the dissipation spectrum the effect of the correction is sufficiently small that an error as large as a factor of two in choosing the probe cut-off (or an appropriate functional form) will affect the dissipation value by <25%.

In Fig. 13, we have fitted to the data the isotropic-turbulence universal spectrum as obtained by Nasmyth (1970). The fit is good, particularly for the 2 cm correction, suggesting that the velocity structure we are measuring is consistent with isotropic turbulence. This is experimental support for using the Eq. (4.2) to calculate the rate of dissipation from the variance of the velocity shear. For other data with

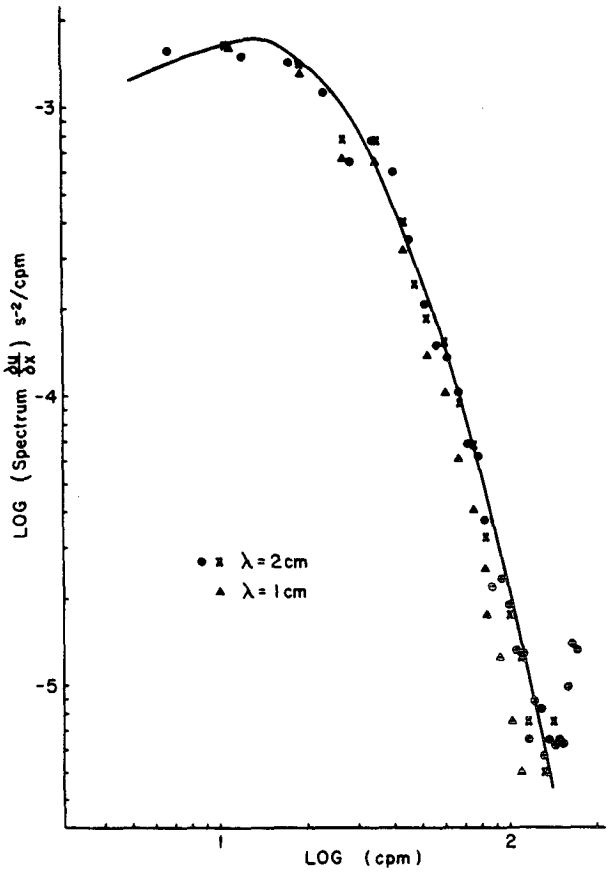

FIG. 13. Velocity-shear spectra for Station 23. The spectra have been corrected for a probe cutoff $\lambda_c = 2$ cm (×, solid circles) and the same data for $\lambda_c = 1$ cm (triangles). The spectra corrected for $\lambda_c = 2$ cm agree well with the isotropic turbulence curve of Nasmyth (1970), shown as a solid line.

lower signal-to-noise ratio, the fit is usually equally good through the reliable data range. Those cases deviating significantly from this form are often of low signal level.

Since we had two shear probes, a comparison can be made between two independently calibrated and analyzed signals that we would expect to be the same on average. This comparison between records from pairs of mutually perpendicular shear probe sensors measuring the dissipation independently but simultaneously is shown in Fig. 14. The straight line representing identical variance is close to our estimate of the ratio between the two determinations of ϵ which has a value of 0.95 ± 0.27. Random errors in the calibration and analysis technique should not contribute an uncertainty >25%. Some of the examples where the difference is as large as a factor of two may be interpreted as real differences from isotropy which can occur between two mutually perpendicular sensors but it is more likely to be due to the statistical nature of the turbulent signal.

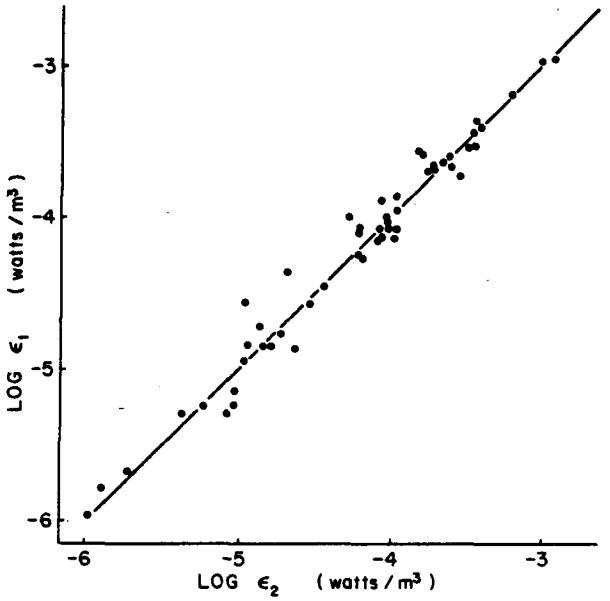

FIG. 14. The dissipation ϵ_1 for sensor number one versus the dissipation determined simultaneously with a second mutually perpendicular sensor, ϵ_2. For each, the dissipation (W m^{-3}) was averaged over a 10 m depth interval. The ratio $\epsilon_1/\epsilon_2 = 1$ is shown as a straight line.

6. Discussion

One of the most interesting features of the data set is the correlation between the atmospheric forcing and the integrated dissipation rate ϵ_I for the mixed layer [Eq. (4.3)]. From one station, the four or five values of ϵ_{lower} (the bottom 10 m of the mixed layer) were averaged to obtain a mean value. In a similar manner, the corresponding values for the upper segment (above the lower segment to 5.5 m depth) were used to obtain an average value of ϵ_{upper} for each station. The time series of these values of ϵ_{upper} and ϵ_{lower} as dissipation per unit volume are shown in Fig. 15. For ϵ_{upper}, values range from 3×10^{-3} W m^{-3} (3×10^{-2} erg cm^{-3} s^{-1}) to 3×10^{-5} W m^{-3}, with the largest values near the beginning of the experiment when the winds were strongest. In the lower mixed-layer segment, values for ϵ_{lower} range from 10^{-3} to 10^{-6} W m^{-3}. Generally, ϵ_{lower} is smaller by at least a factor of two than ϵ_{upper} and there is a tendency for this ratio to be larger towards the end of the experiment, at which time the wind speeds were lower.

Since the data for the top 5.5 m have not been analyzed because of possible contamination from the ship's wake and near-surface vehicle motion we cannot confidently evaluate the integral of Eq. (4.3) to determine the integrated dissipation ϵ_I. There are several equally unsatisfactory choices. We could simply integrate our data from the mixed layer base to a depth of 5.5 m; this result would underestimate the true ϵ_I by a large undetermined amount. We could use a model such as a constant-stress layer to extrapolate our calculated ϵ_I to the surface; then our result would be model dependent. Our choice is to consider that the dissipation in the top 5.5 m is the same as ϵ_{upper}. The equation

$$\epsilon_I = \epsilon_{lower}\Delta Z_{lower} + \epsilon_{upper}(\Delta Z_{upper} + 5.5 \text{ m}) \quad (6.1)$$

has therefore been used to calculate all ϵ_I. These estimates of ϵ_I (W m^{-2}) for the duration of the cruise are shown in Fig. 15 along with the wind speed and mixed-layer depth. An estimate of the error associated with using Eq. (6.1) may be obtained by assuming (A. Gargett, personal communication, 1981) that the mixed layer is a constant-stress boundary layer. The result obtained from (6.1) would be lower by 50% than the value obtained by integrating a logarithmic profile to within a wave amplitude of the surface. Considering the errors associated with the values of ϵ_{lower} and ϵ_{upper} our value of ϵ_I is considered to be known within a factor of two or three. Values range from 4×10^{-2} W m^{-2} near the beginning to 5×10^{-4} W m^{-2} during the period of lower winds. Not shown on the plot are the wind speeds for about three days prior to the experiment, which were light (these were obtained from the weather map surface analysis from the local weather office). The mixed layer depth was ~16 m at the beginning of the study, having remained stable for about a day previously.

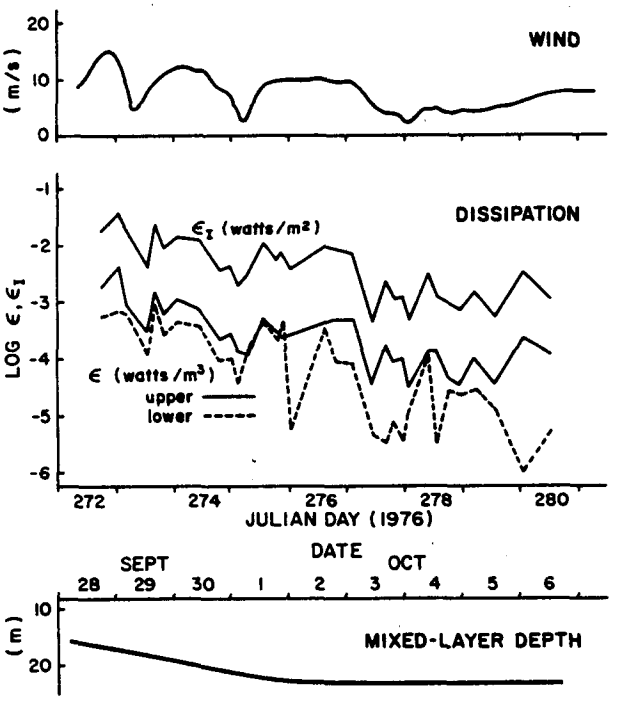

FIG. 15. The wind-speed time series for the 10-day experiment starting on Julian day 272, 28 September 1976. The net dissipation (integrated over the mixed layer) ϵ_I (W m^{-2}) is shown in the center along with the estimates of dissipation per unit volume in the upper and lower mixed layer, ϵ_{upper} and ϵ_{lower} (W m^{-3}). The mixed-layer depth is given at the bottom.

This was followed by variable winds of 2–15 m s^{-1} during which time the mixed layer deepened to 23 m.

The correlation of the dissipation and the atmospheric forcing is presented in Fig. 16, in which ϵ_I is plotted versus U_{10}^3. [It should be noted that the figure is different from that of Oakey and Elliott (1980) because of more recent calibrations of the ship's anemometer (Elliott, 1981).] Each dot represents the average ϵ_I for a half-hour sequence of lowerings; the corresponding wind speed is the average of that which occurred in the hour preceding the start of microstructure observations. Vertical lines join the maximum and minimum values observed in the half-hour sequence. This was chosen to show the range of values rather than a standard deviation with only four or five points.

From Eq. (4.4) one might expect ϵ_I to be proportional to U_{10}^3; the linear regression line of Fig. 16 represents this relationship. As indicated previously, the individual ϵ_I estimates are accurate to about a factor of two or three. The wind speed is accurate to ±20% and therefore ±70% scatter is expected because of the wind-speed error. The point at the lowest wind speed may be anomalously high because of low signal level and attendant signal-to-noise problems, or larger wind-speed error at 2 m s^{-1}. Such effects as buoyancy flux or restratification in the mixed layer may be more important. It should be emphasized that the uncertainty in the mean value of ϵ_I is not the (factor of two or three) uncertainty in the individual measurements but is related as well to the variability of the turbulent field and is improved by the number of independent measurements. It must also be remembered that many of the errors discussed were systematic and not random, and the scatter of Fig. 16 represents only random errors. The relationship shown in Fig. 16 between ϵ_I and U_{10} is given by $\epsilon_I = (U_{10}/38)^3$. The ratio of the mean values of ϵ_I to this line has an RMS scatter of 55% (excluding the lowest wind-speed point). With the uncertainties outlined we assert that we have defined a relationship between the dissipation in the mixed layer and the surface energy flux to about a factor of two. Our data of dissipation per unit mass for the upper layer, ϵ_{upper}, plotted versus U_{10}^3 given a plot similar to Fig. 16 and the regression line can be described as $\epsilon_{upper} = (U_{10}/91)^3$ at a mean depth of 8 m.

One of the few sources of data with which some comparison can be made is that of Stewart and Grant (1962). Their estimate is, however, for ϵ and not ϵ_I. In an examination of their original field data (H. Grant, pers. commun., 1978), it was not possible to identify unequivocally a mixed-layer depth. For some of their data, a choice of 4 m seems reasonable. If this mixed-layer depth is used for their data collected between 1 and 2 m depth for an average wind speed of 7 m s^{-1}, their point (solid square) shown on Fig. 16 falls within the range of scatter of individual ϵ_I. It is higher than our line by a factor of two, and, although the errors are large, this may be an indication of the errors we are encountering by extrapolating the dissipation to the upper 5 m in our determination of ϵ_I.

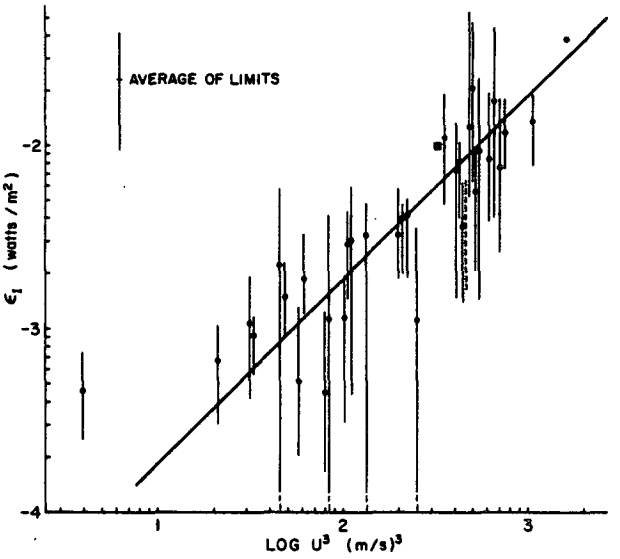

FIG. 16. The dissipation integrated over the mixed layer, ϵ_I (W m^{-2}), versus the cube of the 10 m wind speed, U_{10}^3. Each dot represents the average value obtained for several measurements in one half-hour period; the lines join the maximum and minimum values observed during this period. The "average of limits" (upper left) indicates the mean deviation of maximum and minimum values from the mean. The solid square is from results of Stewart and Grant (1962). The vertical dashed line is from Gargett *et al.* (1979) in the Sargasso Sea. [Note: The abscissa differs from that of Oakey and Elliott (1980) because of corrections applied to U_{10} as a result of shipboard anemometer calibrations.]

More recent data of Gargett *et al.* (1979) from the Sargasso sea show several vertical profiles of velocity microstructure using the instrument CAMEL under a variety of wind–wave conditions. One profile, C3, is associated with winds of 6–10 m s^{-1} following stronger winds associated with a front passing 8 h previously. From their Fig. 3, high levels of dissipation are seen near the surface, which are presumably a result of direct surface wind–wave forcing. Estimating ϵ_I for the upper 50 m from their figure yields a value of $\sim 2.3 \times 10^{-3}$ W m^{-2}. A second region of high dissipation near the base of the mixed layer may have as its source instability associated with inertial wave shear. Including the whole mixed layer in an estimate of ϵ_I yields a value of $\sim 7 \times 10^{-3}$ W m^{-2}. This range of values (from 2 to 7×10^{-3} W m^{-2}) has been plotted as a vertical bar at a mean $U_{10}^3 = 500$ on Fig. 16 for comparison. It shows good agreement with our average line.

The straight-line fit in Fig. 16 indicates that dissipation accounts for a constant fraction of the energy flux E_{10} in the atmospheric boundary layer. This

fraction can be estimated using Eq. 4. For a 10 m s^{-1} wind speed we have

$$E_{10} = \rho_a C_{10} U_{10}^3$$
$$= 1.2 \times 1.3 \times 10^{-3} \times 10^3 = 1.6 \text{ W m}^{-2}.$$

At that wind speed $\epsilon_I \approx 2 \times 10^{-2}$ W m^{-2}, which is $\sim$1% of E_{10}. This is well within the expected range for coupling atmospheric energy to the ocean. It can be compared to values for deepening the mixed layer from Denman and Miyake (1973), who require 0.12% E_{10} to appear as potential energy in deepening the mixed layer or $\sim{}^1/_{10}\epsilon_I$. Remembering that our values of ϵ_I are likely to be underestimated, the dissipation in the mixed layer represents energy larger by at least a factor of 10 than the energy going into deepening.

For this experiment, the energy flux going into the deepening of the mixed layer has not been calculated in detail. As can be seen in Fig. 15, the mixed layer deepened by 5 m from 16 to 21 m in the first three days, deepened more slowly to 23 m in two days and remained essentially at the same depth for the remainder of the experiment. If one considers a simple uniform well-mixed layer of depth h as shown in Fig. 3, deepening an amount δh per unit time t through a density gradient ρ' at the base of the mixed layer (typically $\rho' = 0.2$ kg m^{-4} as shown in Fig. 9), one can estimate the potential energy of deepening from $E_p \approx (\rho' \delta h g h)/(2\rho t)$. For the deepening period, this yields a value (integrated over the mixed layer) of $\sim 5 \times 10^{-3}$ W m^{-2}. If one uses Denman's estimate of 0.12% of energy flux from the wind field going into potential energy of deepening and a wind speed of $U_{10} = 10$ m s^{-1} one obtains a value of 2×10^{-3} W m^{-2}. Considering the simplicity of the present calculation, this indicates that the rate of deepening is consistent with Denman's results. It is not clear, however, what are the effects of advection on the observed deepening.

We have shown in Fig. 16 the correlation between surface stress and the value of ϵ_I. Is ϵ_I directly wind-related? Examining the many profiles of Fig. 12 indicates a higher level of turbulence near the surface, the level decreasing with depth, often with a gap before the mixed-layer base. There is occasionally a burst near the mixed-layer base or at the top of the pycnocline. Only near the beginning does one see fluid actively entrained at the mixed-layer base as shown by the two-sided temperature signals for profiles such as those from stations 21, 23 and 69. In Fig. 8, we saw that there was a persistent density structure (determined mostly by salinity) extending well into the mixed layer. Even in periods of high wind speeds, the mixed layer is not being continually overturned by turbulence generated at the surface. Generation of turbulence, at least in the lower half of the mixed layer, appears to be through shear instability. Over nearly all of the mixed layer the gradient Richardson number, Ri, (averaged over 5 m) is <4 and over large portions is <1, determined in part by a large velocity shear. This Ri may be small enough on average that a large portion of the observed ϵ can be generated through a Richardson-number type of instability. It may well be that the link between surface stress and mixed-layer turbulence is the generation of inertial- and near-inertial-period oscillations as discussed by Pollard (1970) and others more recently. These oscillations are generated efficiently by winds with time scales much less than the inertial period. The decay of these inertial-period oscillations may be due in part to the loss of energy in the generation of turbulence in the mixed layer.

Recently, Bell (1978) has examined the generation of internal waves by the interaction of mixed-layer turbulence advected by near-surface inertial waves over the irregularities at the base of the mixed layer. This mechanism of feeding energy into the internal-wave field causes the decay of inertial-period oscillations generated in the mixed layer by surface winds. For Brunt-Väisällä frequency $N \sim 10^{-2}$ s^{-1}, mixed layer depth $\sim$25 m (similar to our Emerald Basin values) and inertial-current magnitude $\sim$0.25 m s^{-1}, he estimates 3×10^{-3} W m^{-2} (3 erg cm^{-2} s^{-1}) going into the internal-wave field (or considering the errors and assumptions, a range from 1×10^{-3} to 1×10^{-2} W m^{-2}). For our experiment with inertial-current magnitude U_0 of order 0.4 m s^{-1} during periods of high wind speed ($\sim$10 m s^{-1}), this estimate, which depends linearly on U_0, may be somewhat higher but is still of order 10^{-2} W m^{-2}. At a wind speed of 10 m s^{-1} we find an energy dissipation $\epsilon_I \sim 2 \times 10^{-2}$ W m^{-2}. If the source of this turbulent energy is Richardson-number instability extracting energy from the inertial shear, this mechanism may be equally as likely in the decay of inertial-period oscillations as Bell's proposed mechanism of energy going into the internal-wave field.

A final point for discussion is the spatial and temporal variability of the observed turbulent structure in the mixed layer. Fig. 11 shows five successive drops at 4 min intervals (separated spatially by $\sim$50 m). The structure is variable or patchy in depth and perhaps even more variable in time and/or space. A single profile may indicate a dissipation value of $\epsilon(z)$ or ϵ_I which varies from the mean by an order of magnitude. In a mixed-layer study, one would like to form stable estimates of ϵ which can be compared to other terms in the energy balance equation (4.1). If there is a characteristic length and time scale in the generation process, a stable estimate may be achieved for a sufficient number of length scales sampled in one time period. Information on the variability as shown in Fig. 11 is not sufficient to define a suitable averaging process, although it is evident

(and not surprising) that even five profiles in a 25-minute period improve the correlation in such comparisons as ϵ_I versus U_{10}^3 shown in Fig. 16 when compared to that for a single measurement. Further study of horizontal and vertical coherence of microstructure patches must be done so that instruments used to study turbulence in mixed-layer experiments may be employed in a way that allows one to extract a meaningful average—either a sufficient number of vertical profiles in a short time or a suitable horizontal average.

In summary, we have reported in this paper a study of turbulence levels under a variety of wind-wave conditions in a mixed layer for which there is a small persistent large-scale density gradient and a large-scale horizontal-velocity shear in the mixed layer and across the base. We find turbulence levels which are very variable in space and time but which have intensities from two mutually perpendicular simultaneous measurements that are consistent with the assumption of isotropy. Our turbulence spectra agree with a "universal" isotropic-turbulence curve. Average integrated dissipation levels correlate well with the atmospheric forcing. The generation for the observed turbulence is thought to be not through direct surface phenomena such as wave breaking, but from Richardson-number instability in the mixed layer.

REFERENCES

Bell, T. H., 1978: Radiation damping of inertial oscillations in the upper ocean. *J. Fluid Mech.*, **88,** 289–308.

Denman, K. L., 1973: A time dependent model of the upper ocean. *J. Phys. Oceanogr.*, **3,** 173–184.

——, and M. Miyake, 1973: Upper layer modification at ocean station Papa: observations and simulation. *J. Phys. Oceanogr.*, **3,** 185–196.

Elliott, J. A., 1981: Anemometer blockage on CSS Dawson. Bedford Institute of Oceanography, Res. Note No. 1, May 1981 (unpublished) 14 pp.

Dillon, T. M., and D. R. Caldwell, 1980: The Bachelor spectrum and dissipation in the upper ocean. *J. Geophys. Res.*, **85,** 1910–1916.

Gargett, A. E., T. B. Sanford and T. R. Osborn, 1979: Surface mixing layers in the Sargasso Sea. *J. Phys. Oceanogr.*, **9,** 1090–1111.

Garratt, J. R., 1977: Review of drag coefficients over oceans and continents. *Mon. Wea. Rev.*, **105,** 915–929.

Hinze, J. O., 1959: *Turbulence, an Introduction to its Mechanism and Theory.* McGraw-Hill, 586 pp.

Kraus, E. B., 1977: *Modeling and Prediction of the Upper Layers of the Ocean.* Pergamon Press, 325 pp.

Nasmyth, P., 1970: Oceanic turbulence. Ph.D. thesis, Inst. Oceanogr., University of British Columbia, 69 pp.

Niiler, P. P., and E. B. Kraus, 1977: One-dimensional models of the upper ocean. *Modeling and Prediction of the Upper Layers of the Ocean*, E. B. Kraus, Ed., Pergamon Press, 325 pp.

Oakey, N. S., 1977: An instrument to measure oceanic turbulence and microstructure. Bedford Institute of Oceanography, Rep. Ser., BI-R-77-3, 52 pp.

——, and J. A. Elliott, 1980: Dissipation in the mixed layer near Emerald Basin. *Marine Turbulence*, J. C. J. Nihoul, Ed., Elsevier, 123–133.

Osborn, T. R., 1978: Measurement of energy dissipation adjacent to an island. *J. Geophys. Res.*, **83,** 2939–2957.

——, and W. R. Crawford, 1980: An airfoil probe for measuring turbulent velocity fluctuations in water. *Air–Sea Interaction: Instruments and Methods*, F. Dobson, L. Hasse and R. Davis, Eds., Plenum, 369–386.

——, and T. E. Siddon, 1975: Oceanic shear measurements using the airfoil probe. *Proc. Third Biennial Symposium on Turbulence in Liquids*, University of Missouri, Rolla.

Pollard, R. T., 1970: On the generation by winds of inertial waves in the ocean. *Deep-Sea Res.*, **17,** 795–812.

Richman, J., and C. Garrett, 1977: The transfer of energy and momentum by the wind to the surface mixed layer. *J. Phys. Oceanogr.*, **7,** 876–881.

Siddon, T. E., 1971: A miniature turbulence gauge utilizing aerodynamic lift. *Rev. Sci. Instr.*, **42,** 653–656.

Stewart, R. W., and H. L. Grant, 1962: Determination of the rate of dissipation of turbulent energy near the sea surface in the presence of waves. *J. Geophys. Res.*, **67,** 3177–3180.